Clinical Science (2017) **131** 2347–2362
DOI: 10.1042/CS20171006

PORTLAND PRESS

Research Article

Aspirin-triggered resolvin D1 reduces pneumococcal lung infection and inflammation in a viral and bacterial coinfection pneumonia model

Hao Wang[1], Desiree Anthony[1], Selcuk Yatmaz[1], Odilia Wijburg[2], Catherine Satzke[2,3], Bruce Levy[4], Ross Vlahos[1] and Steven Bozinovski[1]

[1]Chronic Infectious and Inflammatory Disease Programme, School of Health and Biomedical Sciences, RMIT University, Bundoora, Australia; [2]Department of Microbiology and Immunology, The Peter Doherty Institute for Infection and Immunity, The University of Melbourne, Melbourne, Australia; [3]Department of Paediatrics, Royal Children's Hospital, Parkville, Victoria, Australia; [4]Department of Medicine, Pulmonary and Critical Care Medicine, Brigham and Women's Hospital and Harvard Medical School, Boston, MA, U.S.A.

Correspondence: Steven Bozinovski (steven.bozinovski@rmit.edu.au)

Formyl peptide receptor 2/lipoxin A_4 (LXA_4) receptor (Fpr2/ALX) co-ordinates the transition from inflammation to resolution during acute infection by binding to distinct ligands including serum amyloid A (SAA) and Resolvin D1 (RvD1). Here, we evaluated the proresolving actions of aspirin-triggered RvD1 (AT-RvD1) in an acute coinfection pneumonia model. Coinfection with *Streptococcus pneumoniae* and influenza A virus (IAV) markedly increased pneumococcal lung load and neutrophilic inflammation during the resolution phase. Fpr2/ALX transcript levels were increased in the lungs of coinfected mice, and immunohistochemistry identified prominent Fpr2/ALX immunoreactivity in bronchial epithelial cells and macrophages. Levels of circulating and lung SAA were also highly increased in coinfected mice. Therapeutic treatment with exogenous AT-RvD1 during the acute phase of infection (day 4–6 post-pneumococcal inoculation) significantly reduced the pneumococcal load. AT-RvD1 also significantly reduced neutrophil elastase (NE) activity and restored total antimicrobial activity in bronchoalveolar lavage (BAL) fluid (BALF) of coinfected mice. Pneumonia severity, as measured by quantitating parenchymal inflammation or alveolitis was significantly reduced with AT-RvD1 treatment, which also reduced the number of infiltrating lung neutrophils and monocytes/macrophages as assessed by flow cytometry. The reduction in distal lung inflammation in AT-RvD1-treated mice was not associated with a significant reduction in inflammatory and chemokine mediators. In summary, we demonstrate that in the coinfection setting, SAA levels were persistently increased and exogenous AT-RvD1 facilitated more rapid clearance of pneumococci in the lungs, while concurrently reducing the severity of pneumonia by limiting excessive leukocyte chemotaxis from the infected bronchioles to distal areas of the lungs.

Introduction

Colonization of the upper respiratory tract with *Streptococcus pneumoniae* (the *Pneumococcus*) provides a reservoir for transmission of the *Pneumococcus* within a population. Colonization of the upper airways is normally confined to this compartment; however *S. pneumoniae* (SP) is the leading cause of bacterial pneumonia and invasive diseases. There are multiple environmental and microbial factors that can facilitate dissemination of *Pneumococcus* from the nasopharyngeal niche to the lower airways [1]. In particular, concurrent respiratory viral infections can transiently compromise host immunity to the *Pneumococcus* [2], as well as increase the density of pneumococcal colonization and severity of disease [3]. Influenza A virus (IAV) also triggers pneumococci to be released from biofilms in a more virulent

Received: 28 April 2017
Revised: 27 July 2017
Accepted: 03 August 2017

Accepted Manuscript Online: 03 August 2017
Version of Record published: 25 August 2017

Clinical Science (2017) **131** 2347–2362
DOI: 10.1042/CS20171006

form [4]. High mortality caused by pandemic strains of IAV has been directly associated with secondary bacterial pneumonia caused by common upper respiratory tract bacteria [5]. The rate of pneumococcal hospitalizations also coincides with the emergence of influenza pandemics [6].

People with underlying chronic lung disease such as chronic obstructive pulmonary disease (COPD) are particularly susceptible to respiratory infections including coinfection with bacterial and viral pathogens [7]. COPD is a major global cause of premature death [8], and respiratory infections commonly trigger acute exacerbations of COPD (AECOPD). Bacterial and viral coinfections during AECOPD are common and can result in more severe exacerbations associated with an increase in pulmonary inflammation [9]. We have previously shown that AECOPD associated with bacterial and viral coinfections result in significantly higher levels of systemic inflammation as determined by the acute phase reactant, serum amyloid A (SAA) [10]. Circulating levels of SAA markedly increase during acute infection where plasma concentrations can increase over 1000-fold. Both viral and bacterial respiratory infections increase the circulating SAA levels that typically peak at 3–5 days following infection and the levels of SAA decline with clinical recovery [11]. In addition to increased circulating levels of SAA during acute infection, we have shown that IAV and the bacterial ligand lipopolysaccharide (LPS) potently stimulate *de novo* synthesis of SAA transcript in the lungs, where SAA synthesis peaked on day 5 and resolved to baseline levels by day 10 in IAV-infected mice [12].

SAA serves pleotropic roles during acute infection including opsonizing Gram-negative bacteria to facilitate more efficient phagocytosis by neutrophils [13]. SAA is also a functional agonist for the formyl peptide receptor 2/lipoxin A_4 (LXA_4) receptor (Fpr2/ALX) where it stimulates leukocyte chemotaxis [14]. Furthermore, we have recently shown that local lung challenge with recombinant SAA potently stimulates neutrophilic inflammation via IL-17A-dependent mechanisms [15,16]. SAA can also promote neutrophil survival by suppressing the apoptotic machinery through activation of ERK and PI3K/Akt signaling pathways [17]. Hence, increased production of SAA during acute infection plays an important protective role involving stimulation of neutrophil and monocyte recruitment, phagocytosis, and survival required for clearance of bacterial pathogens. This process is normally self-limiting with a decline in SAA production during the resolution phase of infection; however, the persistent elevation of SAA may lead to accumulation of neutrophils that can result in excessive lung injury.

The production of specialized proresolving mediators (SPMs) during acute infection can also initiate essential molecular mechanisms that prevent excessive neutrophil recruitment. Resolvin D1 (RvD1) and its aspirin-triggered epimer (aspirin-triggered RvD1 (AT-RvD1)) are generated from the essential π-3 fatty acid, docosahexaenoic acid (DHA) and interact with two known human receptors, namely Fpr2 and DRV1/GPR32 to initiate organ protective properties. Since mice do not express DRV1/GPR32, Fpr2 represents the major receptor for RvD1 in mice. AT-RvD1 is a promising therapeutic target in bacterial pneumonia as it enhanced macrophage phagocytosis of Gram-negative *Escherichia coli* and *Pseudomonas aeruginosa* and accelerated neutrophil efferocytosis during pneumonia to prevent excessive lung injury [18]. AT-RvD1 also promoted more rapid clearance of Gram-negative, non-typeable *Haemophilus influenzae* by stimulating efferocytosis mediated by M2 skewed macrophages [19]. Here, we demonstrate that in our bacterial and viral coinfection model associated with increased neutrophilic inflammation, levels of circulating and lung tissue SAA remained markedly elevated during the resolution phase following pneumococcal infection (7 days post-SP inoculation). Furthermore, delivery of exogenous AT-RvD1 during the acute phase of infection improved clearance of pneumococci in the lungs and reduced pulmonary consolidation caused by excessive recruitment of neutrophils and monocytes during coinfection.

Methods

Animals

Male C57BL/6J mice (8–10 weeks old) from the Animal Resources Centre (Perth, Australia) were housed at $22 \pm 1^{\circ}C$ under normal 12-h light/dark cycle and fed a standard chow and water *ad libitum*. All experiments were approved by the Animal Ethics Committee of RMIT University (AEC #1509) and performed in compliance with the National Health and Medical Research Council (NHMRC) of Australia guidelines. In the coinfection experiment, mice were divided into four groups: SAL (saline), SP, IAV, and SPIAV (coinfected). On day 0 of experiment, mice from SP and SPIAV groups were infected intranasally with SP(serotype: 19F, strain: EF3030, 10^5 colony forming units (CFUs) in 35 μl saline) under light isoflurane anesthesia. On day 1, mice from IAV and SPIAV groups were infected intranasally with IAV (strain: A/HKx31 (H3N2), 10^4 PFU in 30 μl saline). In separate experiments, SAL and SPIAV mice were treated intranasally with AT-RvD1 (17(R)-RvD1, Cayman Chemical, 100 ng in 35 μl saline) or vehicle (1% ethanol in equivalent volume of saline) once daily on day 4 and 6. On day 7, mice were culled by intraperitoneal overdose of sodium pentobarbitone. Bronchoalveolar lavage (BAL) was performed via tracheotomy and total/differential BAL cell counts were determined as previously described [16]. Lung was perfused with ice-cold PBS to remove excess blood.

The right lobe of the lung was immediately excised and kept on ice-cold PBS for flow cytometric analysis. The left lobe was fixed in 10% neutral-buffered formalin for histology and the rest was snap-frozen in liquid nitrogen prior to –80°C storage for further analysis.

Quantitation of SP and IAV

Quantitation of SP in the BAL fluid (BALF) was performed by viable count, where serial dilutions were cultured overnight on selective agar (horse blood agar supplemented with 5 μg/ml gentamicin). In addition, quantitative real-time PCR (qPCR) was used to measure SP and IAV in the lung tissue. Briefly, bacterial DNA and viral RNA were isolated by homogenizing lungs in TRIzol (Life Technologies) using a TissueLyser (Qiagen) in accordance with the manufacturer's instructions. SP DNA qPCR was performed using a commercial kit from Qiagen (Microbial DNA qPCR Assay #330025) as per manufacturer's instructions and bacterial load was determined by using standard curve generated from a known quantity of pneumococci. qPCR on polymerase A (PA) subunit gene of IAV was performed using TaqMan® Fast Virus 1-Step Master Mix as previously described [20]. Viral load was determined by using a standard curve generated from a known quantity of IAV.

Reverse transcriptase quantitative PCR for gene expression analysis

RNA was purified from lung tissue using RNeasy Kit (Qiagen), from which cDNA was prepared using High Capacity cDNA Kit (Life Technologies) as previously described [21]. Reverse transcriptase quantitative PCR (RT-qPCR) was performed using bioinformatically validated Taqman primers/probes (Life Technologies), namely glyceraldehyde phosphate dehydrogenase (*Gapdh*, Mm03302249_g1), interferon-γ (*Ifng*; Mm01168134_m1), Fpr2 (*Fpr2*, Mm00484464_s1), SAA (*Saa1*, Mm00656927_g1), IL-6 (*Il6*, Mm00446190_m1), IL-1β (*Il1*β, Mm00434228_m1), CCL2/MCP1 (*Ccl2*, Mm00441242_m1), and CXCL2/KC (*Cxcl2*, Mm00436450_m1). The threshold cycle values (C_t) were normalized to a reference gene *GAPDH* and the relative fold-change determined by the $\Delta\Delta C_t$ value as previously described [21].

Myeloperoxidase, protein, elastase, and ELISA assays

Myeloperoxidase (MPO) activity was assessed by homogenizing ground lung tissue (50 mg/ml) in extraction buffer (50 mM potassium phosphate monobasic pH 6.0, 0.5% hexadecyltrimethyl ammonium bromide and 10 mM EDTA). Following centrifugation, lung lysate was incubated with reaction buffer (50 mM potassium phosphate monobasic pH 6.0, 0.167 mg/ml *o*-Da (Fast Blue B, Sigma), and 0.005% H_2O_2) and the change in absorbance 460 per minute (3–2min) resulting from decomposition of H_2O_2 and subsequent oxidation of *o*-Da was measured using a CLARIOstar® plate reader. Total protein levels in the BALF were determined by a Pierce BCA Protein Assay Kit (Life Technologies). Neutrophil elastase (NE) activity in BALF as a marker for neutrophil activity was measured using an EnzChek® Elastase Assay Kit (Life Technologies). Briefly, 30 μl of BALF was diluted with 60 μl 1× Reaction Buffer in a 96-well plate, to which 10 μl of 50 μg/ml DQ elastin substrate was added. Reaction was protected from light and incubated at 37°C for 24 h. Fluorescence was then measured using CLARIOstar® (E_x/E_m: 505/515 nm). Lung tissue was homogenized in lysis buffer (150 mM NaCl; 50 mM Tris/HCl pH 7.4; 1% NP-40, 10 μl/mg protease inhibitor cocktail) using a TissueLyser (Qiagen) and lysates were collected for determination of protein lung levels. SAA levels in the lung lysate, serum, and BALF were measured using a SAA Mouse ELISA Kit (Life Technologies) and RvD1 levels were determined using commercial ELISA Kit (Cayman Chemical) according to the manufacturer's instructions. The lung tissue lysate was also used to determine IL-1β and IL-6 protein levels in the lung using commercial ELISA assays (Life Technologies).

SP susceptibility assay

BALF was centrifuged and cell-free aliquots were archived at –80°C and subjected to freeze-thaw cycle prior to use in this assay. Total antimicrobial activity in the BALF was determined using an SP susceptibility assay as previously described [22]. Briefly, 114 μl of SP (3×10^6 CFU/ml) cultured in Todd–Hewitt broth (THB, BD Biosciences) was incubated with 6 μl of BALF from mice at 37°C for 4 h in a 5% CO_2 incubator. Serial dilutions of the culture were incubated overnight on selective agar (horse blood agar supplemented with 5 μg/ml gentamicin) and colonies were counted to assess bacterial growth rate in the presence of BALF.

Flow cytometric assessment of immune cells in lung

Single-cell suspension preparation and flow cytometric analysis were performed as previously described [16]. Inhibition of non-antigen binding of immunoglobulins to Fc receptors was performed using a rat anti-mouse CD16/CD32

Clinical Science (2017) **131** 2347–2362
DOI: 10.1042/CS20171006

antibody (BD Biosciences). A strict gating strategy was used to determine different immune cell populations and propidium iodide was used to exclude dead cells. Neutrophils and macrophages were gated as single, live cells with intermediate or high expression of FSC-A and SSC-A, which displayed these cells as a distinct cluster compared with lymphocytes and myeloid cells. In addition, neutrophils were classified as $CD45^{Hi}$, $F4/80^{-/Low}$, and $Ly6G^{+}$ whereas macrophages were classified as $CD45^{Hi}$, $F4/80^{Hi}$, and $Ly6G^{-}$. For macrophage subpopulations, alveolar macrophages were classified as $CD11b^{Low}$, $CD11c^{Hi}$; exudative macrophages were classified as $CD11b^{Hi}$, $CD11c^{Hi}$; infiltrating macrophages were classified as $CD11b^{Hi}$, $CD11c^{Low}$. Lymphocytes were labeled with fluorochrome–conjugated antibodies against CD3 and CD8 used at preoptimized dilutions in order to differentiate and quantitate the number of $CD3^{+}CD8^{+}$ T cells. Cells were analyzed on a BD FACSCanto II (BD Biosciences) and data were analyzed using FlowJo software (FlowJo LLC, Oregon, U.S.A.). All anti-mouse antibodies were purchased from BD Biosciences, namely FITC–conjugated CD45, PB–conjugated F4/80, PE/Cy7–conjugated CD11c, APC–conjugated CD11b, APC/Cy7–conjugated Ly6G.

Histology and immunohistochemistry

The left lobe of lung fixed in 10% neutral-buffered formalin was processed, paraffin-embedded, and sectioned at thickness of 5 μm. Histologic examination was performed on Hematoxylin and Eosin (H&E)-stained sections of the left lung using a slide scanner to capture the entire lobe (Olympus VS120). Airway inflammation in H&E sections were blindly graded and the average of five individual airways was presented as previously described [23]. Parenchymal inflammation or pneumonia (area of alveolar infiltrate minus airways/vessels) was graded using the following criteria across the entire lobe: 1 = mild, inflammatory cells sporadically present in parenchyma; 2 = moderate, single inflammatory lesion accounting for up to 10% lung parenchyma, 3 = severe, multiple inflammatory lesions or pneumonia sites accounting for 10–50% lung parenchyma, 4 = complete, multiple inflammatory lesions and diffused consolidation or pneumonia accounting for >50% lung parenchyma. Immunohistochemical staining for Fpr2 was performed by incubating with Fpr2 antibody (NLS1878, Novus Biologicals, 1:300) overnight at 4°C, followed by secondary antibody (biotinylated goat anti-rabbit IgG, Vector Laboratories, 1:200, 1 h) and avidin–biotin horseradish peroxidase (HRP) complex (Vector Elite kit; Vector Laboratories, 1:200, 1 h). Staining was developed in freshly prepared 3,3′-Diaminobenzidine (DAB) solution and sections were then counterstained in hematoxylin. Images were captured using the Olympus VS120 slide scanner.

Data analysis

Data are presented as the mean ± S.E.M. All data were statistically analyzed using GraphPad Prism 6.0 (GraphPad, San Diego, CA). Where detailed and appropriate, two-tailed Student's *t* tests, one-way or two-way ANOVA with Dunnett or Bonferroni's post hoc tests were used. $P<0.05$ was considered to be statistically significant.

Results

Coinfection augments bacterial lung load and inflammation during resolution phase

Schematic representation of the coinfection model is presented in Figure 1A, where mice were inoculated intranasally with a 19F strain of SP or SAL on day 0, followed by IAV or SAL infection on day 1. To determine the chronicity of SP lung infection in this model, bacterial load in the BALF and the lung was assessed 7 days post pneumococcal inoculation (Figure 1B,C). In mice infected with SP alone, day 7 represents resolution of infection as residual pneumococcal numbers (<100 CFUs) remained in the BALF with none detected in the lung tissue. Coinfection with IAV resulted in markedly higher pneumococcal lung infection, evident by the high bacterial load in both the BALF and the lung (Figure 1B,C). IAV lung viral titers were not altered by coinfection (Figure 1D) and the increase in IFN-γ levels by IAV was not altered by coinfection ($P>0.05$, Figure 1E).

Pneumonia caused by coinfection increases lung elastase activity and edema

The cellular inflammatory response to SP and/or IAV infection was assessed by analyzing the BAL compartment. The inflammatory response in mice inoculated with SP alone resolved by day 7 as no difference in leukocytes' numbers was seen as compared with SAL-treated mice (Figure 2A–C). There was a significant increase in BAL macrophages in IAV-infected mice and this was not significantly altered by coinfection (Figure 2B). BAL neutrophil numbers were increased in IAV-infected mice on day 7, and this was further increased in coinfected mice by approximately 100%

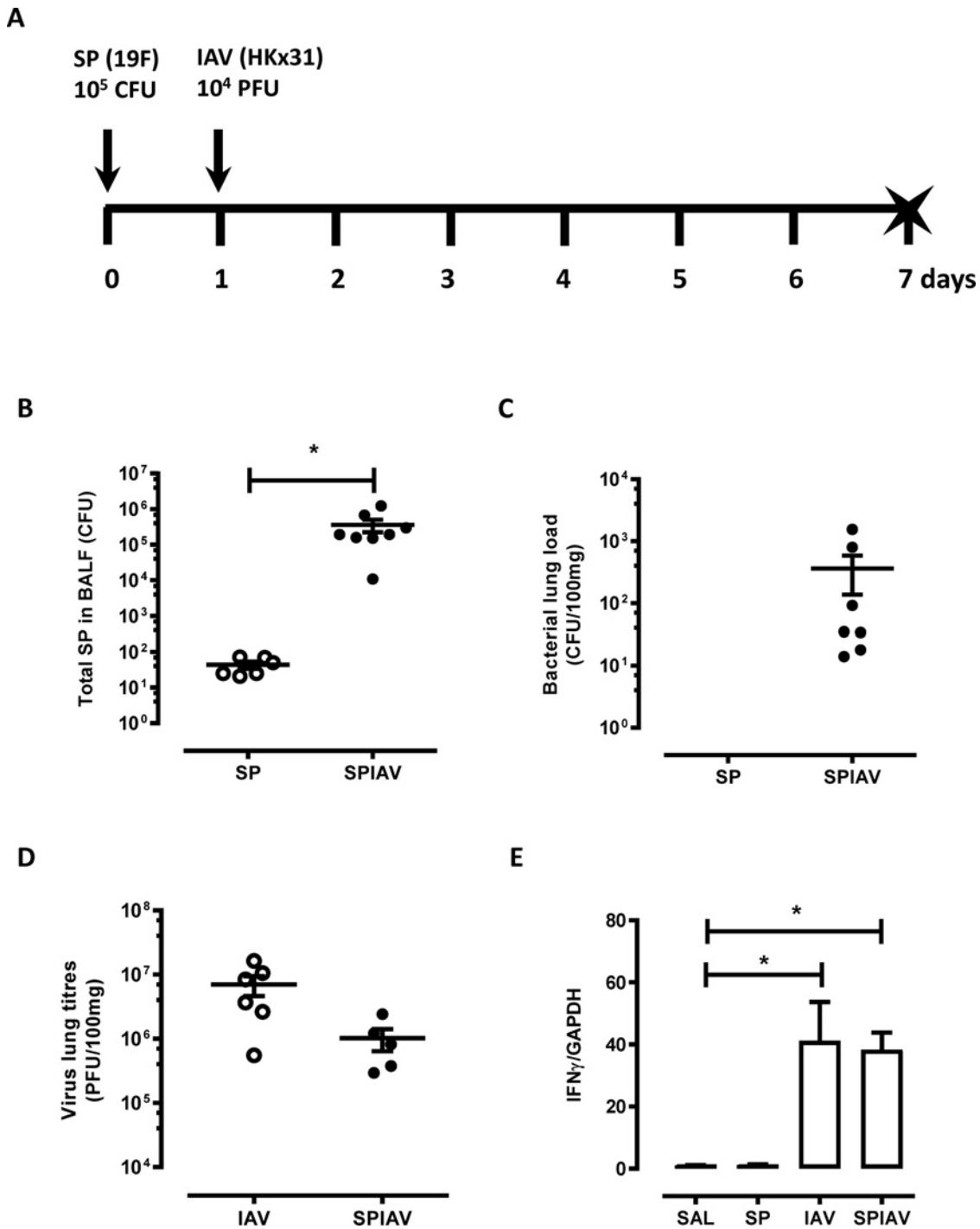

Figure 1. Coinfection increases pneumococcal lung infection

(**A**) Schematic representation of the experimental protocol and the timing of inoculation with SP and/or IAV. Mice were infected intranasally with SP (serotype 19F/strain EF3030, 10^5 CFU) and/or IAV (strain HKx31, H3N2, 10^4 PFU). On day 7, mice were culled and outcomes were measured. SP load was assessed in both BALF and lung tissue. (**B**) Freshly collected BALF was serially diluted and incubated on horse blood agar supplemented with 5 μg/ml gentamicin overnight at 37°C and CFUs were recorded from highest countable dilution (n=6–8). *P<0.05, two-tailed Student's t tests. (**C**) Lung tissue that had been snap-frozen was homogenized and microbial DNA extracted, and qPCR performed to quantitate SP levels. (**D**) qPCR on viral RNA extracted from lung tissue was performed to quantify IAV levels. (**E**) Taqman qPCR was performed on lung mRNA extraction for assessment of *IFNγ* gene expression. n=5–10, *P<0.05, one way ANOVA compared with SAL.

Clinical Science (2017) **131** 2347–2362
DOI: 10.1042/CS20171006

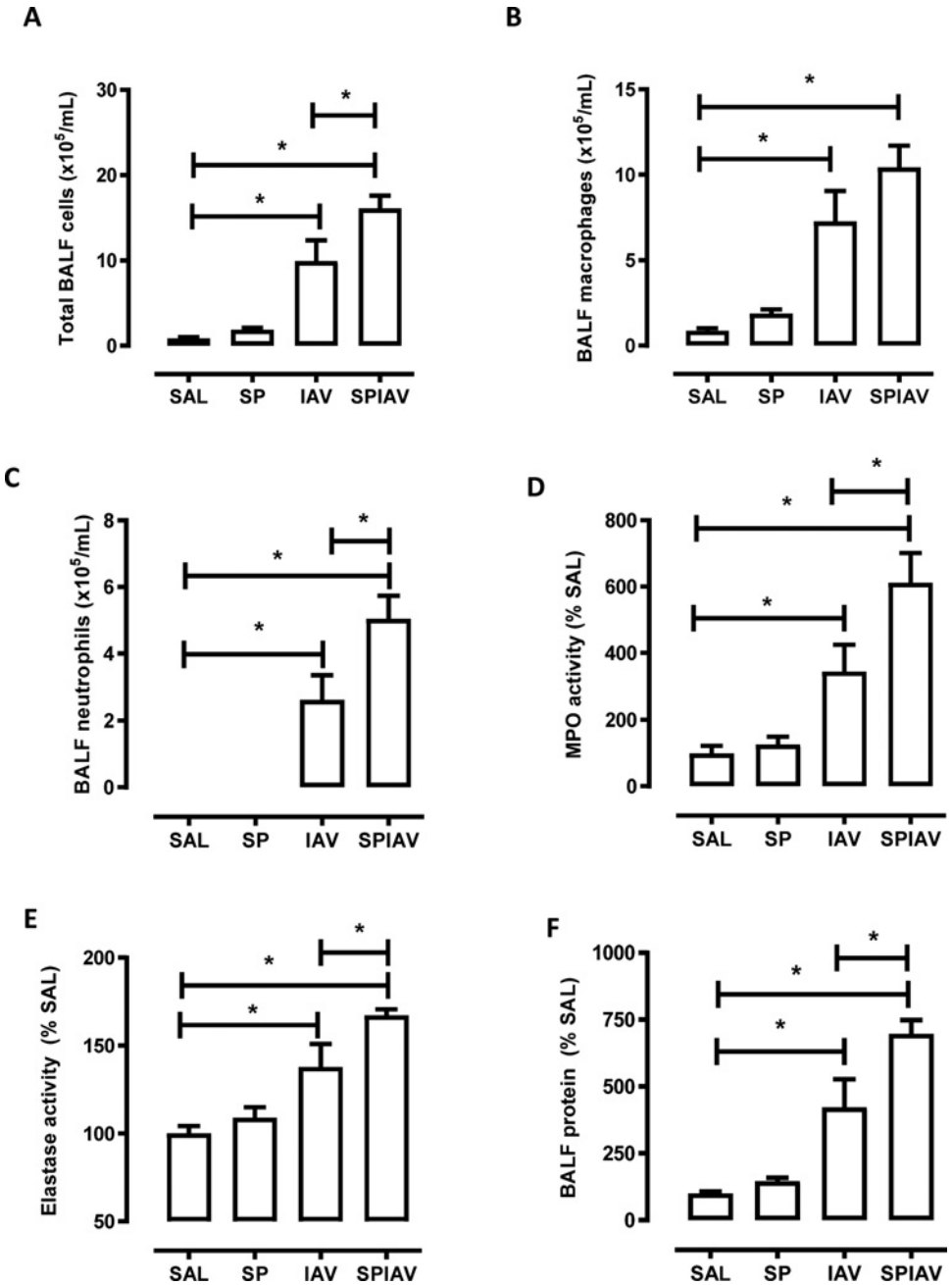

Figure 2. Coinfection increases neutrophilic inflammation and edema caused by IAV

(**A**) Total cells from BAL were assessed by viability counting and cytospins were prepared for the assessment of (**B**) macrophages and (**C**) neutrophils' numbers. (**D**) Neutrophil MPO activity in lung tissue was measured as an indicator for neutrophil numbers in the lung tissue. (**E**) NE activity in the BALF was measured as a marker for neutrophil degranulation and (**F**) total proteins in the BALF was measured to assess degree of lung edema in the lung. n=5–8, *P<0.05, one-way ANOVA compared with SAL or IAV as indicated.

(Figure 2C). MPO activity was assessed on lung tissue and in concordance with BAL neutrophil counts, elevated MPO activity in the lungs of IAV-infected mice increased by approximately 80% in coinfection (Figure 2D). To assess neutrophil activation, NE released into the BALF was measured (Figure 2E). Similar to the MPO activity results, IAV infection significantly increased NE activity, which was further elevated by SP coinfection by 20%. Consistent with increased NE proteolytic activity contributing to edema during acute infection and inflammation, total BALF protein levels were increased in IAV-infected mice and this was significantly higher in coinfected mice (Figure 2F).

Clinical Science (2017) **131** 2347–2362
DOI: 10.1042/CS20171006

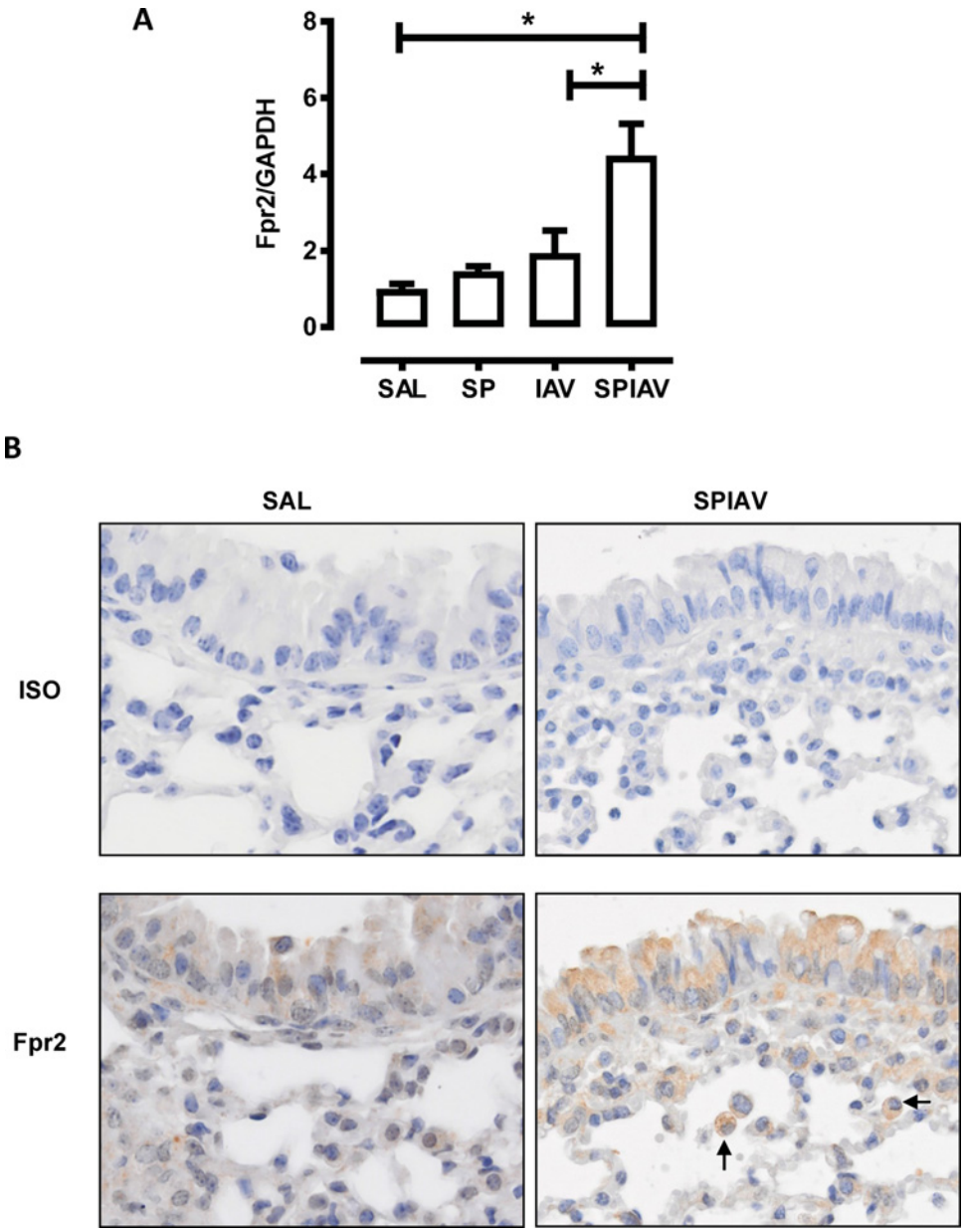

Figure 3. Coinfection increases Fpr2 transcipt expression and immunoreactivity in the lungs

(**A**) Fpr2 transcript levels were assessed in the lungs by Taqman RT-qPCR demonstrating a significant increase in coinfected mice. (**B**) Fpr2 immunoreactivity was determined by immunohistochemistry on lung sections from SAL and coinfected (SPIAV) mice, demonstrating prominent bronchial epithelial staining and the presence of $Fpr2^{+}$ lung macrophages in coinfected mice. The black arrows indicate lung macrophages. *$P<0.05$, one-way ANOVA compared with SAL or IAV as indicated.

SAA and Fpr2 are markedly increased in the lungs of coinfected mice

Expression of Fpr2 on lung tissue on day 7 following pneumococcal inoculation was determined by qPCR, where levels of Fpr2 were significantly elevated in coinfected mice relative to SAL- or IAV-treated mice (Figure 3A). Immunoreactive Fpr2 protein was detected by immunohistochemistry (Figure 3B); where modest Fpr2 immunoreactivity was mainly limited to bronchial epithelial cells in the lungs of SAL-treated control mice. In coinfected mice, Fpr2 immunoreactivity was much more prominent in bronchial epithelium and macrophages. We next evaluated expression of the inflammatory Fpr2 agonist, SAA. *SAA* mRNA levels were elevated by IAV infection (four-fold, relative to SAL control) and this was further increased (nine-fold relative to SAL control, $P<0.05$ compared with IAV) by coinfection (Figure 4A). SAA protein levels in lung homogenate were also increased in IAV-infected mice compared with

Clinical Science (2017) **131** 2347–2362
DOI: 10.1042/CS20171006

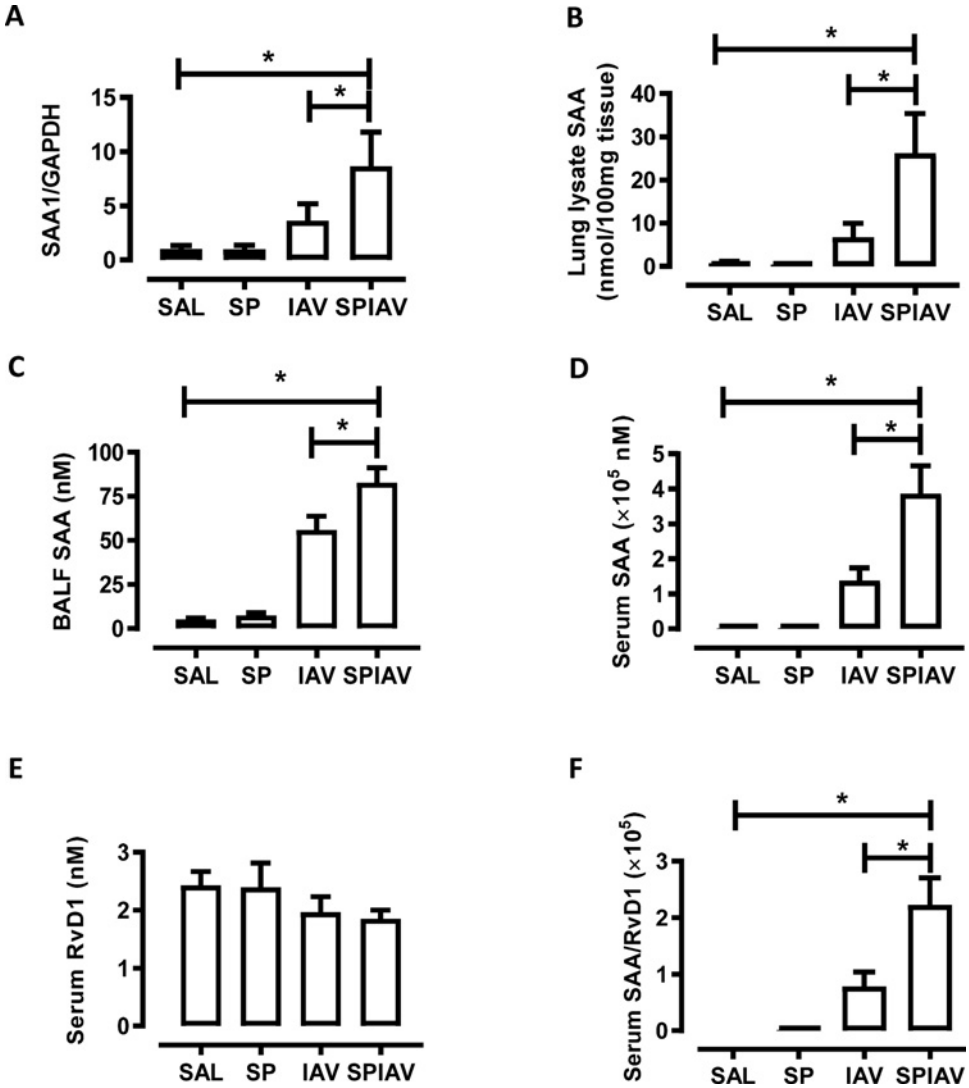

Figure 4. Coinfection markedly increased circulating and tissue SAA levels

(**A**) Gene expression of SAA was measured in the lung by Taqman RT-qPCR. (**B**) SAA protein in the lung homogenate lysate, (**C**) BALF, and (**D**) serum was measured by ELISA. (**E**) RvD1 levels in the serum was measured by ELISA. (**F**) The relative ratio of SAA/RvD1 was determined for the matching serum samples. n=6–10, *P<0.05, one-way ANOVA compared with SAL or IAV as indicated.

SAL control mice (Figure 4B, IAV; 6.7 nmol compared with SAL; 0.22 nmol/100 mg tissue) and levels significantly increased further in coinfected mice (SPIAV; 26.2 nmol/100 mg, P<0.05 compared with IAV). A similar pattern of SAA protein expression was detected in BALF and serum, where IAV increased SAA levels and this was further elevated in the coinfection setting (Figures 4C,D). In addition, levels of the SPM, RvD1 were measured in the serum. Serum RvD1 levels were not altered by either single infections or coinfection on day 7 (Figure 4E, P>0.05), and the ratio of SAA relative to RvD1 in serum was markedly elevated in coinfected mice (Figure 4F, P<0.05). Levels of RvD1 in BALF and lung homogenate were below the limit of detection for this assay.

AT-RvD1 reduces pneumococcal lung load and alveolitis in coinfected mice

We next explored the therapeutic effect of exogenous AT-RvD1 in our coinfection model, where coinfected mice were treated intranasally with AT-RvD1 or vehicle once daily on day 4 and day 6 as summarized in Figure 5A. On day 7, SP load was assessed in the BALF and the lung, demonstrating a significant 70% reduction in pneumococcal load in BALF (Figure 5B) and lung (Figure 5C) following AT-RvD1 treatment. AT-RvD1 did not significantly alter lung

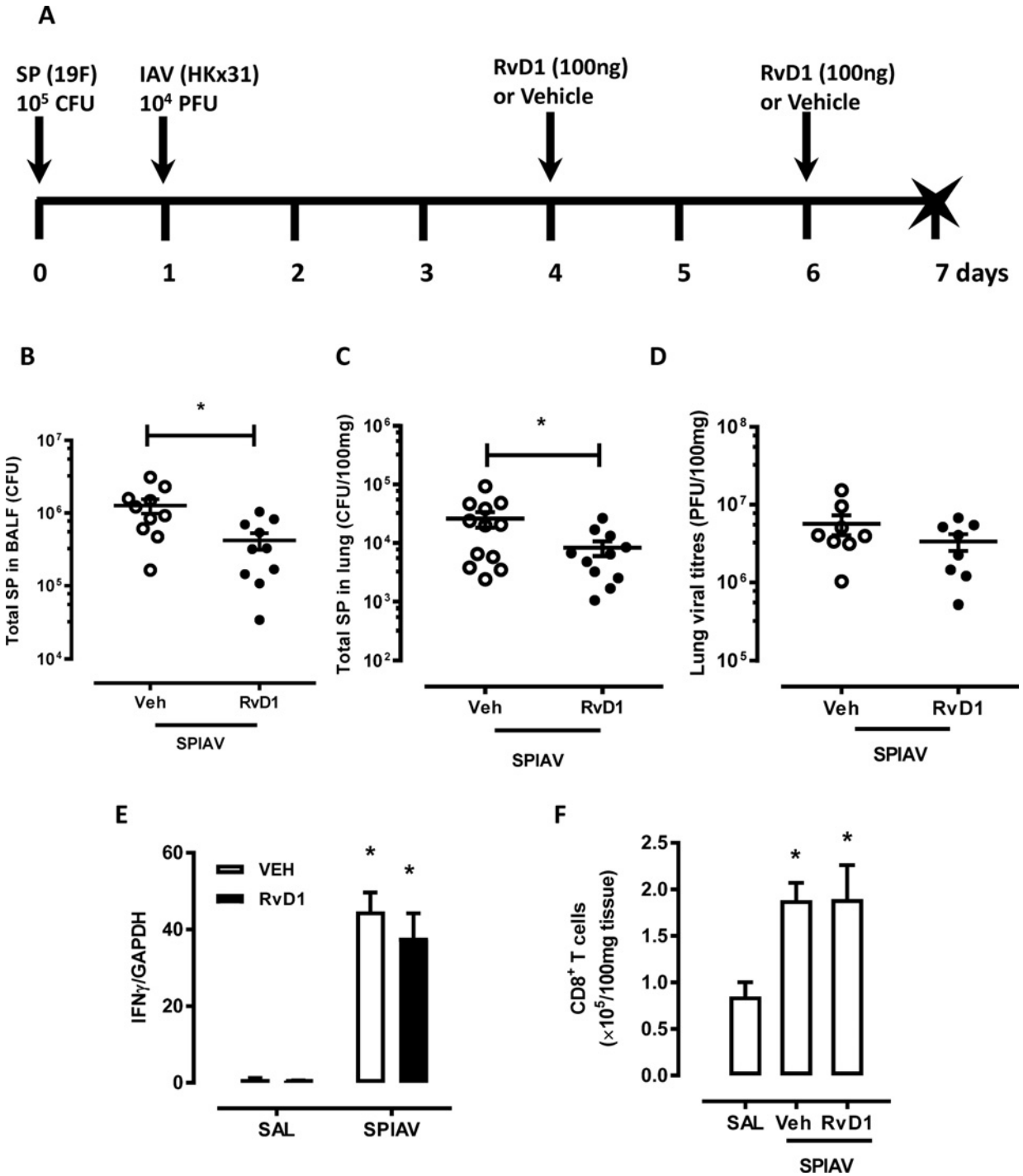

Figure 5. AT-RvD1 treatment reduces bacterial load in the lung

(**A**) Mice were infected with SP on day 0 and IAV on day 1 as described in Figure 1A. On days 4 and 6, mice were treated intranasally with AT-RvD1 (SPIAV-RvD1) or vehicle (SPIAV-Veh) once daily. On day 7, mice were culled and outcomes were measured. (**B**) Freshly collected BALF was serially diluted and incubated on horse blood agar supplemented with 5 μg/ml gentamicin overnight at 37°C and CFUs were recorded from highest countable dilution. (**C**) Lung tissue that had been snap-frozen was homogenized and microbial DNA qPCR was carried out to quantitate SP levels. (**D**) qPCR on viral RNA extracted from lung tissue was performed to quantitate IAV levels. (**E**) Taqman qPCR was performed on lung mRNA extraction for assessment of *IFNγ* gene expression. (**F**) $CD8^+$ T cells in the lungs were determined by flow cytometry, demonstrating an increase in $CD8^+$ numbers in coinfected mice that was not altered by AT-RvD1. n=5–12, $^*P<0.05$, two-tailed Student's t tests.

Clinical Science (2017) **131** 2347–2362
DOI: 10.1042/CS20171006

viral titers (Figure 5D), IFN-γ as determined by RT-qPCR (Figure 5E) or numbers of lung $CD8^+$ T cells in coinfected mice, as determined by flow cytometry (Figure 5F). To assess the airway and parenchymal inflammation/alveolitis, H&E-stained lung sections were scored blinded as described in the 'Methods' section using whole slide scanned images of the left lung lobe. Representative images of the entire lobe (left panels) and 200× magnification of areas of interest (right panels) are shown in Figure 6A. Quantitative evaluation of parenchymal inflammation or alveolitis demonstrated that AT-RvD1 significantly reduced pulmonary consolidation in coinfected mice (Figure 6B), whereas bronchial or airway inflammation was not significantly altered (Figure 6C).

Neutrophil staining of lung immune cells demonstrated that lung neutrophil numbers increased in coinfected mice and this was significantly reduced by AT-RvD1 treatment by approximately 50% (Figure 7A,B). The attenuated neutrophil influx after AT-RvD1 treatment was also consistent with a 30% reduction in MPO activity in the lung (Figure 7C) and 50% reduction in the neutrophil counts in the BALF (Figure 7D). Total NE activity in the BALF of coinfected mice increased two-fold relative to SAL-treated mice, and AT-RvD1 treatment significantly reduced elastase activity by approximately 13% (Figure 7E). In addition, the total antimicrobial activity was assessed by culturing SP in the presence of BALF. The *in vitro* pneumococcal growth rate increased by 60% in cultures incubated with BALF from coinfected mice relative to control mice (Figure 7F). The BALF from AT-RvD1 treated coinfected mice significantly reduced pneumococcal growth by approximately 20% (compared with vehicle treated coinfected mice, $P<0.05$; Figure 7F).

In addition, analysis of the macrophage subpopulations (representative macrophage subsets shown in Figure 8A) revealed no changes in alveolar macrophages Figure 8B), but a marked recruitment of exudative ($CD11b^{Hi}$, $CD11c^{Hi}$) and infiltrating monocytes/macrophages ($CD11b^{Hi}$, $CD11c^{Low}$) in the lungs of coinfected mice (Figure 8C,D). AT-RvD1 treatment did not alter alveolar macrophage ($CD11b^{Low}$, $CD11c^{Hi}$) or exudative macrophage numbers, but did result in ∼50% reduction in infiltrating monocytes/macrophage numbers (Figure 8B–D). To determine whether AT-RvD1 reduced neutrophil/monocyte numbers through inhibition of inflammatory cytokines and chemokines, we measured IL-1β and IL-6 transcript and protein levels in the lungs. The data show that both inflammatory cytokines were markedly increased in coinfected lungs, but transcript or protein levels were not significantly reduced by AT-RvD1 (Supplementary Figure S1A–D). A very similar pattern of expression was seen for the neutrophil chemokine CXCL2 and the monocyte chemokine CCL2/MCP1, where elevated transcript levels were not significantly reduced by AT-RvD1 (Supplementary Figure S1E,F). In addition, elevated transcript levels of SAA and Fpr2 were not significantly reduced by AT-RvD1 (Supplementary Figure S1G,H).

Discussion

Infection with the 19F strain SP alone was self-limiting and resolved within 7 days. In contrast, acute viral (IAV) infection caused significant lung inflammation at day 7 and in the coinfection model, markedly compromised SP clearance, leading to a further significant increase in lung leukocytes. In the present study, we demonstrate that global Fpr2 lung expression is significantly increased in coinfected mice. Murine Fpr2 is known to be expressed on neutrophils and monocytes/macrophages, and acute injury increases Fpr2 expression in normal bronchial epithelial cells via COX-2-dependent manner [24]. Consistent with these findings, we observed prominent Fpr2 immunoreactivity in the bronchial epithelium and macrophages of coinfected mice. In addition, SAA protein was markedly elevated in the BALF and serum of coinfected mice, where circulating SAA is predominantly synthesized by the liver in response to the 'spill over' of inflammatory mediators from the infected/inflamed site. SAA is a potent chemotactic factor that mediates migration of leukocytes [14] and can also promote expression of proinflammatory mediators under *in vitro* [25] and *in vivo* conditions [12]. We have previously shown that SAA induces a proinflammatory macrophage phenotype [26] that stimulated acute neutrophilic lung inflammation in an Fpr2-dependent manner [16].

Importantly, SAA can oppose the organ protective and proresolving actions of LXA_4, RvD1, and their aspirin-triggered epimers that facilitate the resolution of inflammation via FPR2/ALX in the absence of SAA [12,24,27]. Our approach to reduce excessive neutrophil and monocyte inflammation in coinfected mice was to therapeutically deliver exogenous AT-RvD1 during the acute phase of infection. Fpr2 is the main receptor for AT-RvD1 in mice, which reduces neutrophilic inflammation in response to Gram-negative infection [18,19]. Our data demonstrate that AT-RvD1 potently reduces neutrophil and monocyte numbers in the lungs of coinfected mice, thereby significantly limiting the degree of pneumonia. The organ protective actions of RvD1 analogs include inhibition of neutrophil migration along a chemotactic gradient [28]; hence AT-RvD1 can directly oppose leukocyte movement from the infected bronchi into the distal lung. Interestingly, our histological findings show that parenchymal inflammation or alveolitis is reduced by AT-RvD1, whereas bronchial inflammation was not significantly reduced at this time point, suggesting that alveolar inflammation was cleared more rapidly than bronchial inflammation. We also

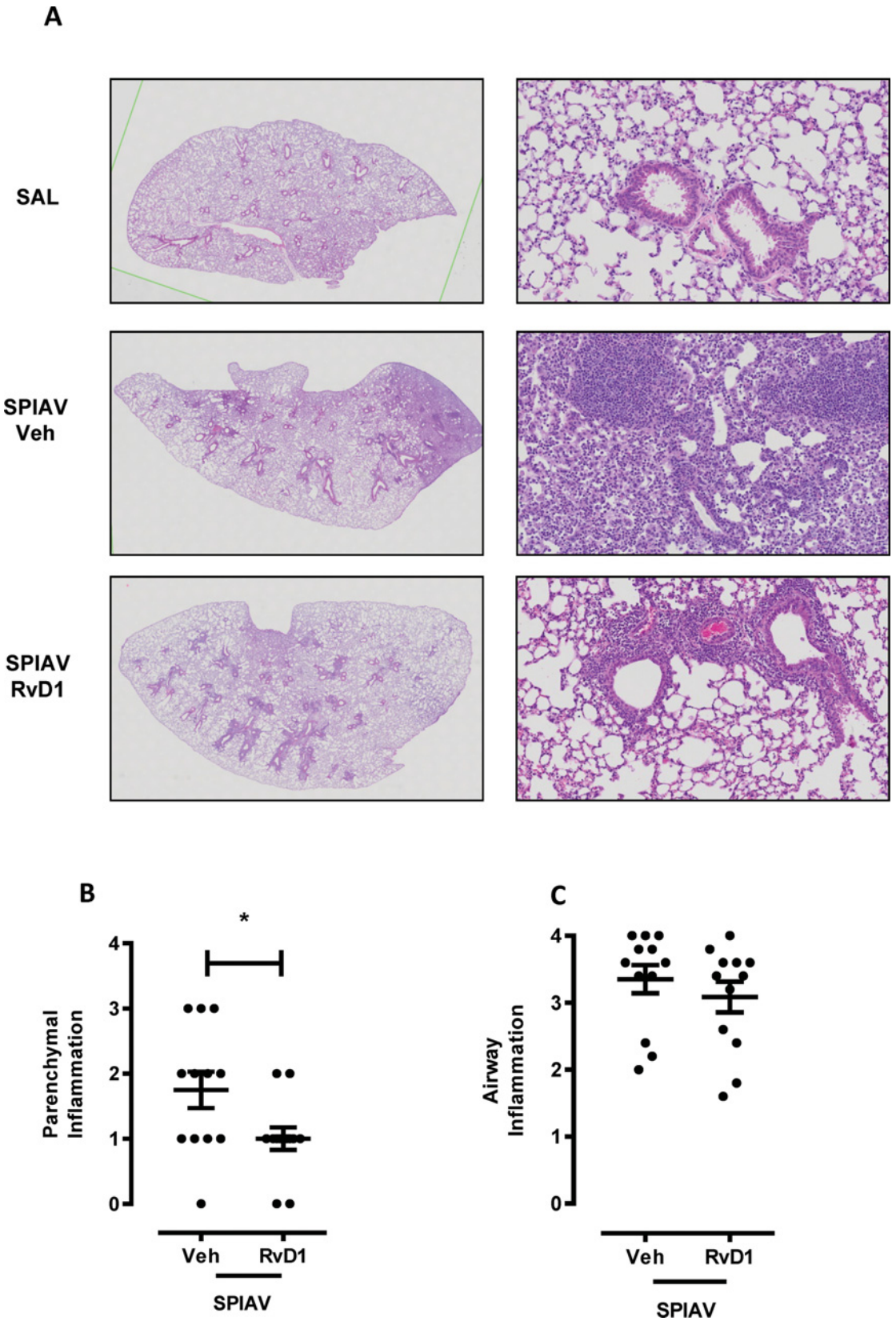

Figure 6. AT-RvD1 treatment ameliorates degree of pneumonia in the lung

(**A**) Representative images of whole slide scan and 200× optical zoom using H&E-stained lung sections. Degree of parenchymal inflammation (**B**) and airway inflammation (**C**) were scored blinded as detailed in the 'Methods' section. n=10–12, $^*P<0.05$, two-tailed Student's t tests.

Clinical Science (2017) **131** 2347–2362
DOI: 10.1042/CS20171006

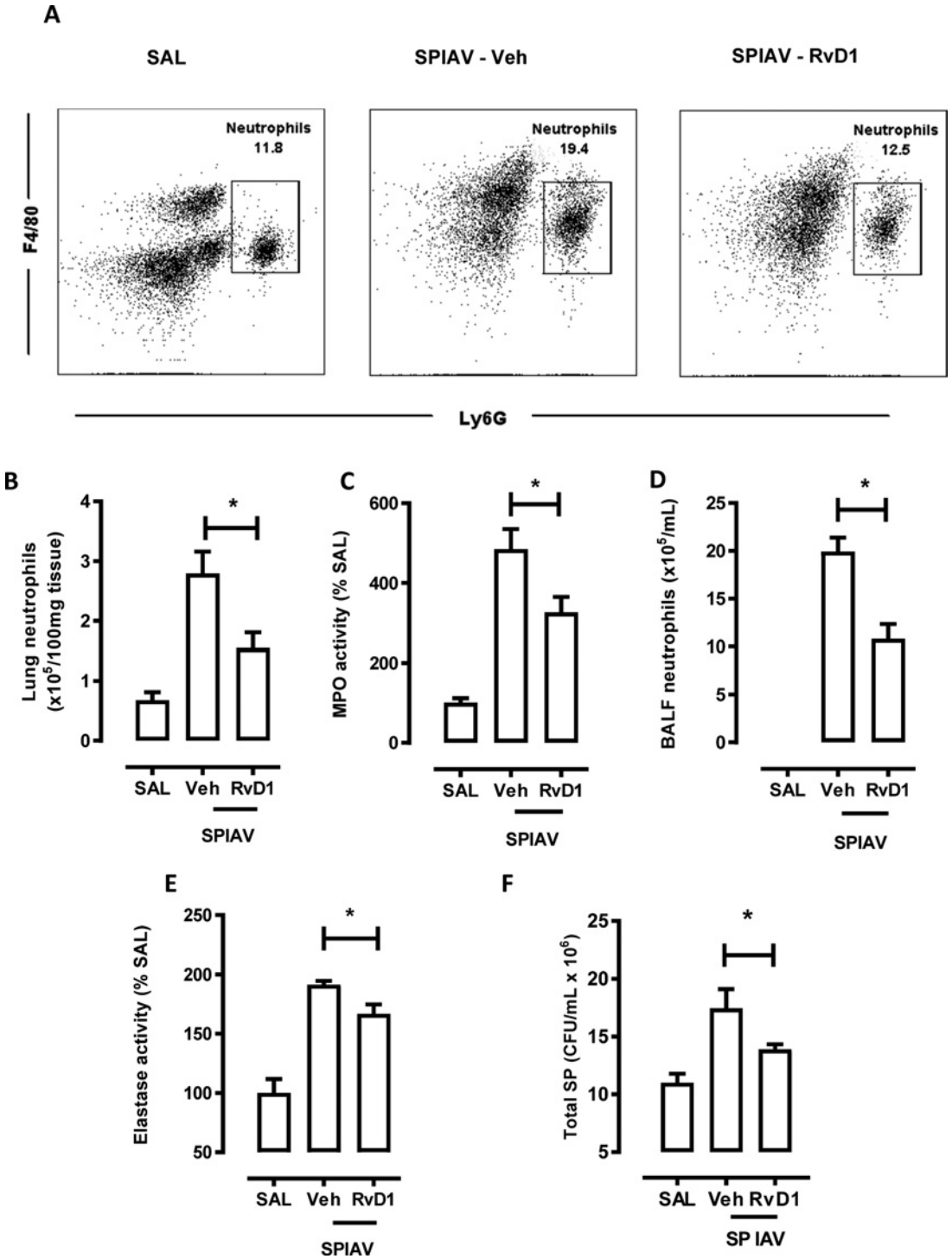

Figure 7. AT-RvD1 (RvD1) treatment reduced neutrophilic inflammation in the lung

Single-cell suspensions were prepared from lung homogenates. Flow cytometric analysis was performed and (**A**) representative flow cytometry dot plots from lung homogenates gated on neutrophils ($F4/80^{-/Low}$, $Ly6G^{+}$). Neutrophil numbers (**B**) in the lung demonstrated a marked increase in coinfected mice and a significant reduction with AT-resolvin D1 treatment. (**C**) Increased neutrophil MPO activity in the lung (**D**) and increased BAL neutrophil numbers were also redcued by AT-RvD1 treatment. (**E**) NE activity in the BALF was also assessed, demonstrating an increase in coinfected mice that was reduced by AT-RvD1. (**F**) Total antimicrobial activity in the BALF was determined using the SP susceptibility assay as described in the 'Methods' section. *In vitro* bacterial growth was increased in the presence of BAL fluid from coinfected mice (compared with SAL), and bacterial growth was significantly lower in cultures containing BALF from AT-RvD1 treated mice (compared with SPIAV-Veh). *$P<0.05$, one-way ANOVA compared with SPIAV-Veh as indicated.

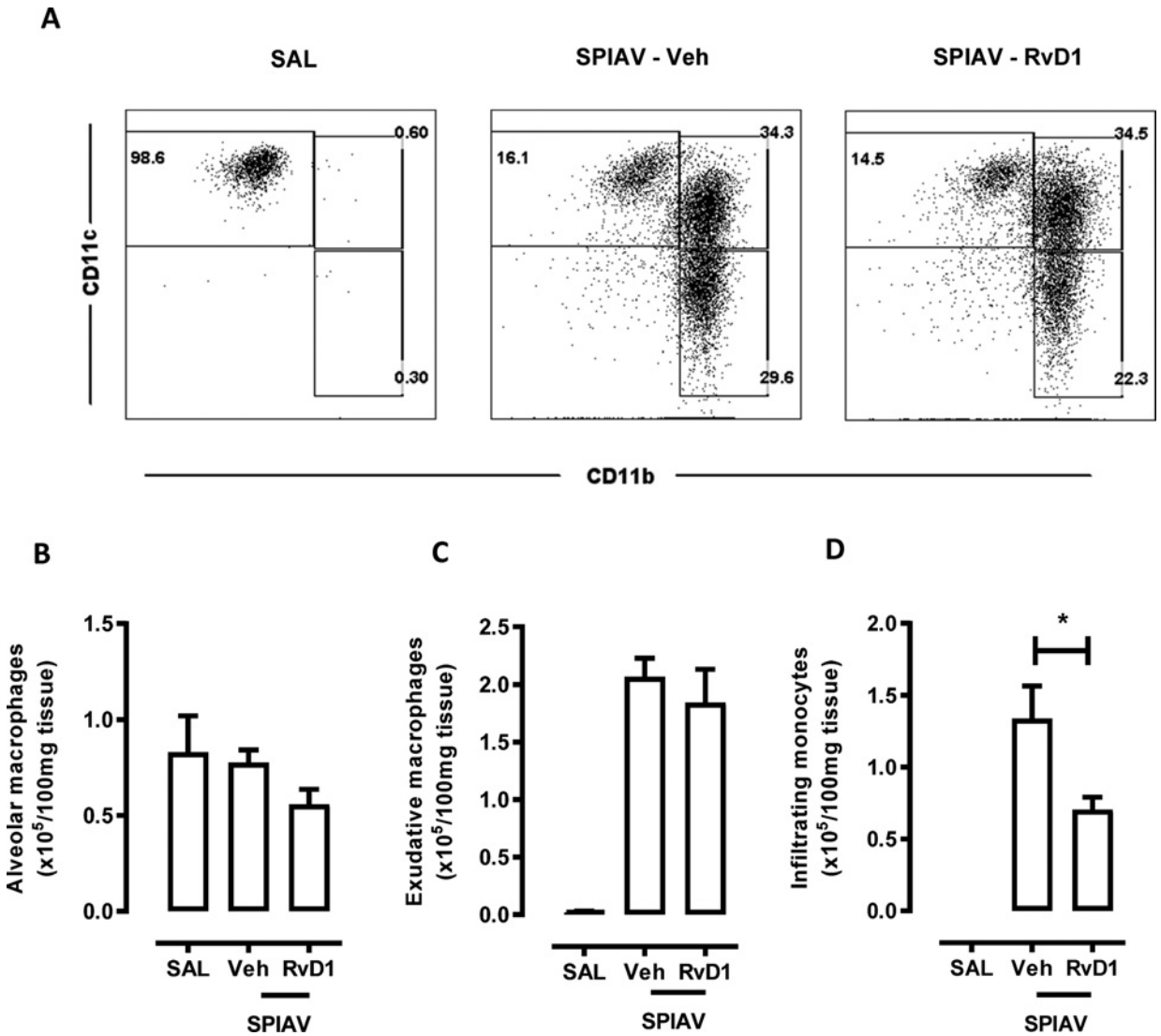

Figure 8. AT-RvD1 treatment reduces infiltrating monocyte recruitment

(**A**) Representative flow cytometry dot plots from lung homogenates gated on macrophage subsets including alveolar macrophages classified as $CD11b^{Low}$, $CD11c^{Hi}$; exudative macrophages classified as $CD11b^{Hi}$, $CD11c^{Hi}$; infiltrating macrophage classified as $CD11b^{Hi}$, $CD11c^{Low}$. Macrophage subsets numbers of (**B**) alveolar macrophages, (**C**) exudative macrophages, and (**D**) infiltrating monocytes/macrophages were determined, demonstrating a significant reduction in infiltrating monocytes as a result of AT-RvD1 treatment (SPIAV-RvD1), $^*P<0.05$, one-way ANOVA compared with SPIAV-Veh as indicated.

observed that AT-RvD1 did not significantly reduce expression of the leukocyte chemokines CXCL2 or MCP-1, nor did it significantly reduce SAA or Fpr2 levels in coinfected mice. Hence, our data strongly suggest that AT-RvD1 primarily halts neutrophil and monocyte migration from the infected bronchioles into the distal alveoli by directly opposing chemotaxis toward inflammatory chemokines.

In addition, AT-RvD1 also stimulated pneumococcal lung clearance, hence would limit the spread of this pathogen into the distal airways and therefore, limit alveolitis exacerbated by coinfection. We found that NE activity was highest in coinfected mice and this was associated with a significant reduction in global antimicrobial activity in the BALF, as the *in vitro* pneumococcal growth rate was highest in bacterial cultures spiked with coinfected BALF. Excessive NE is known to compromise immunity to bacteria by degrading antmicrobial peptides in the BAL compartment leading to impaired bacterial clearance [29]. Importantly, AT-RvD1 significantly reduced NE activity and concurrently restored antimicrobial activity in the BALF of coinfected mice. Our data are consistent with the known actions of AT-RvD1,

Clinical Science (2017) **131** 2347–2362
DOI: 10.1042/CS20171006

which can stimulate the production of the antibacterial peptide lipocalin 2, thereby enhancing bacterial clearance in the lung [18].

We also evaluated the antiviral $CD8^+$ T-cell response in AT-RvD1 treated mice. Consistent with IFN-γ levels, viral infection in coinfected mice increased the number of $CD8^+$ T cells in the lung and this response was not altered by AT-RvD1. Hence, we clearly demonstrate that AT-RvD1 does not compromise viral immunity, but does reduce pneumonia by limiting neutrophil and monocyte chemotaxis and improving bacterial clearance. Acute bacterial infections will also promote the robust recruitment of blood monocytes to restore lung macrophage numbers through maturation of recruited blood monocytes [30]. However, excessive monocyte recruitment can stimulate a secondary phase of neutrophil migration that perpetuates acute lung injury [31]. Since AT-RvD1 potently reduced monocyte recruitment in coinfected mice, this will also reduce the secondary phase of neutrophil recruitment.

Acute immune responses to bacteria and viruses will also promote macrophage phenotypic heterogeneity in the lung [30]. Inoculation of mice with pandemic IAV strains can dramatically deplete resident alveolar macrophages in a temporal manner [32] with gradual restoration of lung macrophages through self-renewal proliferative mechanisms [33]. Significantly, this temporal depletion of lung alveolar macrophages can create a window of opportunity for pathogens such as SP to cause marked increase in pneumococcal outgrowth and lethal pneumonia [32]. At our resolution time point (day 7), we observed robust recruitment of infiltrating monocytes and increased numbers of exudative macrophages in coinfected mice. Furthermore, exudative macrophages were not reduced by AT-RvD1 in our model. This lung macrophage population is particularly important to resolution processes as RvD1 stimulates exudative macrophages to clear apoptotic neutrophils [18].

In summary, our findings demonstrate that coinfection leads to a significant increase in lung edema associated with excessive NE activity and as a consequence, levels of the acute phase reactant SAA are markedly elevated in the BAL and lung compartment. Since SAA can directly target Fpr2 to stimulate neutrophilic inflammation, AT-RvD1 was administered locally into the lungs to initiate resolution of inflammation. AT-RvD1 promoted resolution of inflammation by improving pneumococcal lung clearance, which is compromised in the coinfection setting. Furthermore, AT-RvD1 initiated organ protective effects by limiting exuberant neutrophil and monocyte recruitment. AT-RvD1 represents a novel therapeutic option to reduce the burden of bacterial pneumonia that is exacerbated as a consequence of acute viral infections.

Clinical perspectives

- Uncontrolled and persistent bacterial infection in the lungs of people suffering from acute influenza infection is a key element that promotes severe pneumonia and mortality. Hence, there is a need to develop novel therapies that can concurrently reduce damaging lung inflammation and improve bacterial lung clearance in the coinfection setting.

- In the present study, SAA levels were markedly increased in the lungs of coinfected mice. Since SAA is a functional inflammatory agonist for the formyl peptide receptor 2 (Fpr2), we have evaluated the therapeutic efficacy of an alternative Fpr2 proresolution agonist. AT-RvD1 significantly reduced pneumococcal lung load and severity of pneumonia in coinfected mice.

- The present study provided novel insight into the mechanisms that drive excessive inflammation in the coinfection setting and for the first time, identify AT-RvD1 as an important therapeutic agent in this polymicrobial setting.

Acknowledgements

We thank Hoai Buu Ngo for his technical assistance and Patrick Reading for providing virus stocks.

Author contribution

S.B. and H.W. conceived and conducted the study, and wrote the paper. H.W., S.B., D.A. and S.Y. performed the experiments. C.S., O.W., R.V., B.L. and D.A. assisted in data analysis and interpretation. All co-authors provided intellectual input and critical edited the paper.

Funding

This work was supported by the National Health and Medical Research Council of Australia [grant number APP1067547]; the Australian Research Council [grant number FT130100654]; and the U.S.A. National Institutes of Health [grant number P01-GM095467].

Competing interests

The authors declare that there are no competing interests associated with the manuscript.

Abbreviations

AECOPD, acute exacerbation of chronic obstructive pulmonary disease; AT-RvD1, aspirin-triggered resolvin D1; BAL, bronchoalveolar lavage; BALF, bronchoalveolar lavage fluid; CFU, colony forming unit; COPD, chronic obstructive pulmonary disease; Cox-2, cyclooxygenase-2; Fpr2/ALX, formyl peptide receptor 2/lipoxin A_4 receptor; H&E, Hematoxylin and Eosin; IAV, influenza A virus; IL-17A, Interleukin-17A; INF-γ, Interferon-gamma; LXA_4, lipoxin A_4; MPO, myeloperoxidase; NE, neutrophil elastase; PFU, plaque forming units; qPCR, quantitative real-time PCR; RT-qPCR, reverse transcriptase quantitative PCR; RvD1, Resolvin D1; SAA, serum amyloid A; SAL, saline; SP, *Streptococcus pneumoniae*; SPIAV, *S. pneumoniae* influenza A virus; SPM, specialized proresolving mediator.

References

1 Diavatopoulos, D.A., Short, K.R., Price, J.T., Wilksch, J.J., Brown, L.E., Briles, D.E. et al. (2010) Influenza A virus facilitates *Streptococcus pneumoniae* transmission and disease. *FASEB J.* **24**, 1789–1798
2 McCullers, J.A. (2014) The co-pathogenesis of influenza viruses with bacteria in the lung. *Nat. Rev. Microbiol.* **12**, 252–262
3 Vu, H.T., Yoshida, L.M., Suzuki, M., Nguyen, H.A., Nguyen, C.D., Nguyen, A.T. et al. (2011) Association between nasopharyngeal load of *Streptococcus pneumoniae*, viral coinfection, and radiologically confirmed pneumonia in Vietnamese children. *Pediatr. Infect. Dis. J.* **30**, 11–18
4 Pettigrew, M.M., Marks, L.R., Kong, Y., Gent, J.F., Roche-Hakansson, H. and Hakansson, A.P. (2014) Dynamic changes in the *Streptococcus pneumoniae* transcriptome during transition from biofilm formation to invasive disease upon influenza A virus infection. *Infect Immun.* **82**, 4607–4619
5 Morens, D.M., Taubenberger, J.K. and Fauci, A.S. (2008) Predominant role of bacterial pneumonia as a cause of death in pandemic influenza: implications for pandemic influenza preparedness. *J. Infect. Dis.* **198**, 962–970
6 Weinberger, D.M., Simonsen, L., Jordan, R., Steiner, C., Miller, M. and Viboud, C. (2012) Impact of the 2009 influenza pandemic on pneumococcal pneumonia hospitalizations in the United States. *J. Infect. Dis.* **205**, 458–465
7 Wilkinson, T.M., Hurst, J.R., Perera, W.R., Wilks, M., Donaldson, G.C. and Wedzicha, J.A. (2006) Effect of interactions between lower airway bacterial and rhinoviral infection in exacerbations of COPD. *Chest* **129**, 317–324
8 Jemal, A., Ward, E., Hao, Y. and Thun, M. (2005) Trends in the leading causes of death in the United States, 1970-2002. *JAMA* **294**, 1255–1259
9 Papi, A., Bellettato, C.M., Braccioni, F., Romagnoli, M., Casolari, P., Caramori, G. et al. (2006) Infections and airway inflammation in chronic obstructive pulmonary disease severe exacerbations. *Am. J. Respir. Crit. Care Med.* **173**, 1114–1121
10 Bozinovski, S., Hutchinson, A., Thompson, M., Macgregor, L., Black, J., Giannakis, E. et al. (2008) Serum amyloid a is a biomarker of acute exacerbations of chronic obstructive pulmonary disease. *Am. J. Respir. Crit. Care Med.* **177**, 269–278
11 Whicher, J.T., Chambers, R.E., Higginson, J., Nashef, L. and Higgins, P.G. (1985) Acute phase response of serum amyloid A protein and C reactive protein to the common cold and influenza. *J. Clin. Pathol.* **38**, 312–316
12 Bozinovski, S., Uddin, M., Vlahos, R., Thompson, M., McQualter, J.L., Merritt, A.S. et al. (2012) Serum amyloid A opposes lipoxin A(4) to mediate glucocorticoid refractory lung inflammation in chronic obstructive pulmonary disease. *Proc. Natl. Acad. Sci. U.S.A.* **109**, 935–940
13 Shah, C., Hari-Dass, R. and Raynes, J.G. (2006) Serum amyloid A is an innate immune opsonin for Gram-negative bacteria. *Blood* **108**, 1751–1757
14 Su, S.B., Gong, W., Gao, J.L., Shen, W., Murphy, P.M., Oppenheim, J.J. et al. (1999) A seven-transmembrane, G protein-coupled receptor, FPRL1, mediates the chemotactic activity of serum amyloid A for human phagocytic cells. *J. Exp. Med.* **189**, 395–402
15 Anthony, D., McQualter, J.L., Bishara, M., Lim, E.X., Yatmaz, S., Seow, H.J. et al. (2014) SAA drives proinflammatory heterotypic macrophage differentiation in the lung via CSF-1R-dependent signaling. *FASEB J.* **28**, 3867–3877
16 Anthony, D., Seow, H.J., Uddin, M., Thompson, M., Dousha, L., Vlahos, R. et al. (2013) Serum amyloid A promotes lung neutrophilia by increasing IL-17A levels in the mucosa and $\gamma\delta$ T cells. *Am. J. Respir. Crit. Care Med.* **188**, 179–186
17 El Kebir, D., Jozsef, L., Khreiss, T., Pan, W., Petasis, N.A., Serhan, C.N. et al. (2007) Aspirin-triggered lipoxins override the apoptosis-delaying action of serum amyloid A in human neutrophils: a novel mechanism for resolution of inflammation. *J. Immunol.* **179**, 616–622
18 Abdulnour, R.E., Sham, H.P., Douda, D.N., Colas, R.A., Dalli, J., Bai, Y. et al. (2016) Aspirin-triggered resolvin D1 is produced during self-resolving gram-negative bacterial pneumonia and regulates host immune responses for the resolution of lung inflammation. *Mucosal Immunol.* **9**, 1278–1287
19 Croasdell, A., Lacy, S.H., Thatcher, T.H., Sime, P.J. and Phipps, R.P. (2016) Resolvin D1 dampens pulmonary inflammation and promotes clearance of nontypeable *Haemophilus influenzae*. *J. Immunol.* **196**, 2742–2752
20 Tate, M.D., Ioannidis, L.J., Croker, B., Brown, L.E., Brooks, A.G. and Reading, P.C. (2011) The role of neutrophils during mild and severe influenza virus infections of mice. *PLoS ONE* **6**, e17618
21 Bozinovski, S., Vlahos, R., Zhang, Y., Lah, L.C., Seow, H.J., Mansell, A. et al. (2011) Carbonylation caused by cigarette smoke extract is associated with defective macrophage immunity. *Am. J. Respir. Cell. Mol. Biol.* **45**, 229–236

Clinical Science (2017) **131** 2347–2362
DOI: 10.1042/CS20171006

22 Habets, M.G., Rozen, D.E. and Brockhurst, M.A. (2012) Variation in *Streptococcus pneumoniae* susceptibility to human antimicrobial peptides may mediate intraspecific competition. *Proc. Biol. Sci.* **279**, 3803–3811
23 Coomes, S.M., Kannan, Y., Pelly, V.S., Entwistle, L.J., Guidi, R., Perez-Lloret, J. et al. (2016) $CD4^+$ Th2 cells are directly regulated by IL-10 during allergic airway inflammation. *Mucosal Immunol.* **10**, 150–161
24 Bonnans, C., Fukunaga, K., Levy, M.A. and Levy, B.D. (2006) Lipoxin A(4) regulates bronchial epithelial cell responses to acid injury. *Am. J. Pathol.* **168**, 1064–1072
25 He, R., Sang, H. and Ye, R.D. (2003) Serum amyloid A induces IL-8 secretion through a G protein-coupled receptor, FPRL1/LXA4R. *Blood* **101**, 1572–1581
26 Anthony, D., McQualter, J.L., Bishara, M., Lim, E.X., Yatmaz, S., Seow, H.J. et al. (2014) SAA drives proinflammatory heterotypic macrophage differentiation in the lung via CSF-1R-dependent signaling. *FASEB J.* **28**, 3867–3877
27 Eickmeier, O., Seki, H., Haworth, O., Hilberath, J.N., Gao, F., Uddin, M. et al. (2013) Aspirin-triggered resolvin D1 reduces mucosal inflammation and promotes resolution in a murine model of acute lung injury. *Mucosal Immunol.* **6**, 256–266
28 Kasuga, K., Yang, R., Porter, T.F., Agrawal, N., Petasis, N.A., Irimia, D. et al. (2008) Rapid appearance of resolvin precursors in inflammatory exudates: novel mechanisms in resolution. *J. Immunol.* **181**, 8677–8687
29 Mallia, P., Footitt, J., Sotero, R., Jepson, A., Contoli, M., Trujillo-Torralbo, M.B. et al. (2012) Rhinovirus infection induces degradation of antimicrobial peptides and secondary bacterial infection in chronic obstructive pulmonary disease. *Am. J. Respir. Crit. Care Med.* **186**, 1117–1124
30 Duan, M., Li, W.C., Vlahos, R., Maxwell, M.J., Anderson, G.P. and Hibbs, M.L. (2012) Distinct macrophage subpopulations characterize acute infection and chronic inflammatory lung disease. *J. Immunol.* **189**, 946–955
31 Dhaliwal, K., Scholefield, E., Ferenbach, D., Gibbons, M., Duffin, R., Dorward, D.A. et al. (2012) Monocytes control second-phase neutrophil emigration in established lipopolysaccharide-induced murine lung injury. *Am. J. Respir. Crit. Care Med.* **186**, 514–524
32 Ghoneim, H.E., Thomas, P.G. and McCullers, J.A. (2013) Depletion of alveolar macrophages during influenza infection facilitates bacterial superinfections. *J. Immunol.* **191**, 1250–1259
33 Hashimoto, D., Chow, A., Noizat, C., Teo, P., Beasley, M.B., Leboeuf, M. et al. (2013) Tissue-resident macrophages self-maintain locally throughout adult life with minimal contribution from circulating monocytes. *Immunity* **38**, 792–804